Dust and Snow Cover on Saturn's Icy Moons

Alice Le Gall, Richard D. West, Léa Bonnefoy

Geophysical Research Letters

RESEARCH LETTER
10.1029/2019GL084218

Dust and Snow Cover on Saturn's Icy Moons

A. Le Gall[1], R. D. West[2], and L. E. Bonnefoy[1,3]

[1]LATMOS/IPSL, UVSQ Université Paris-Saclay, Sorbonne Université, CNRS, Paris, France, [2]Jet Propulsion Laboratory, California Institute of Technology, Pasadena, CA, USA, [3]LESIA, Observatoire de Paris, PSL-Research University, CNRS, Sorbonne Université, Université Paris-Diderot, Paris, France

Key Points:
- The final analysis of Cassini radar observations of Saturn's icy moons gives insights into the degree of purity of the regolith
- Saturn innermost moons are extremely radar-bright partly due to the deposition of ultraclean water ice particles from Enceladus' geysers
- The high radar albedos of Saturn inner moons also imply the presence of especially efficient retroreflecting structures in their subsurface

Supporting Information:
- Supporting Information S1

Correspondence to:
A. Le Gall,
alice.legall@latmos.ipsl.fr

Citation:
Le Gall, A., West, R. D., & Bonnefoy, L. E. (2019). Dust and snow cover on saturn's icy moons. *Geophysical Research Letters*, *46*, 11,747–11,755. https://doi.org/10.1029/2019GL084218

Received 22 JUN 2019
Accepted 13 OCT 2019
Accepted article online 23 OCT 2019
Published online 6 NOV 2019

Abstract The final analysis of the Cassini radar observations of Saturn's icy moons presented here shows that the exchange of material between the planet's dust rings and moons, which is specific to the Saturnian system, plays a key role in the current state of the airless satellite regolith. Far from Saturn, the vast debris ring from Phoebe progressively coats the leading side of Iapetus with optically dark material reducing its radar brightness. On the contrary, close to the planet, the extreme radar brightness of the innermost moons Mimas, Enceladus, and Tethys (that exceeds that of the Galilean satellites) is most likely related to Enceladus's geysers and the E-ring which brings ultraclean water ice to their surfaces. The measured radar albedos and observed hemispheric dichotomies require at least a few decimeters thick "snow" cover and that the near surfaces of Saturn's innermost moons contain especially efficient backscattering structures whose nature remains an outstanding problem.

Plain Language Summary From 2004 to 2017, the Cassini spacecraft explored Saturn's family of moons which, Titan excepted, are devoid of atmosphere. As such, these moons are not protected against the effects of bombardment by grains of various origins which alter their surface composition and texture. Cassini radar observations can help assess these effects by giving insights into the purity of the satellites' water ice. Indeed, when the RADAR sends waves toward a surface made of a transparent medium such as pure water ice, the waves penetrate into the ground down to few meters and have therefore more opportunities to bounce on buried structures and return to the spacecraft to be recorded. Inversely, "dirty" surfaces appear radar-dark. Cassini radar observations support the idea that the dark deposit on Iapetus's leading face originates from Phoebe's ring and is a few decimeters thick. On the other hand, closer to Saturn, the E-ring (fed by Enceladus's geysers) acts as a snow cannon, depositing fresh water ice particles onto Enceladus and its neighbors. These satellites are radar-brighter than Galilean moons because their surfaces are cleaner and also contain structures especially efficient at returning waves to the spacecraft. The nature of these "boomerang" structures is still unknown.

1. Introduction

On 15 September 2017, the Cassini spacecraft plunged into Saturn and burned up in its atmosphere. This fatal dive marked the end of a 13.5-year-long fruitful mission dedicated to the exploration of the Saturn system. In particular, the Cassini mission has revolutionized our understanding of Saturn's airless moons providing dramatic images of their surfaces and evidence of past, and even present, geological activity on Dione and Enceladus, respectively (Porco et al., 2006).

Even if most of Saturn's icy satellites were likely formed from the same planetary subnebula and are composed largely of water ice (e.g., Clark et al., 1986), they show a variety of surface features that are a testimony to their divergent evolution. Their respective thermal history and near environment have led to regoliths with different compositions and structures that contain a record of the exogenic and endogenic processes, which have shaped them. Microwaves can help access this record as demonstrated by the first analyses of the data collected by the RADAR on board the Cassini spacecraft (Ostro et al., 2006, 2010).

While it was initially designed to examine the surface of Titan through the veil of its opaque atmosphere, the Cassini RADAR was occasionally used to observe Saturn's airless moons, namely, the six intermediate-sized satellites (in order of distance to Saturn) Mimas, Enceladus, Tethys, Dione, Rhea, and Iapetus, and the two irregular-shaped satellites Hyperion and Phoebe. Probing their subsurface at a wavelength of 2.2 cm (13.8 GHz), the instrument opened a new dimension in the exploration of these moons.

Except for a few data sets collected during targeted flybys (Le Gall et al., 2014; Ostro et al., 2006, 2010; Ries & Janssen, 2015; Wye, 2011), all icy satellite observations by the Cassini RADAR were distant. They typically occurred at ranges between 50,000 and 500,000 km where the antenna beam width was comparable to or greater than the apparent angular extent of the target's disk. They were thus mainly designed for measuring the disk-integrated 2.2-cm radar albedo (in the active mode) and brightness temperature (in the passive mode). Nevertheless, they provide insights into the intervariations and intravariations of the thermal, physical, and compositional properties of Saturn's satellites and thus into the unique story of each of these objects.

In this paper, we expand upon the work of Ostro et al. (2006, 2010) as the observation database has increased (and will not increase anymore) and a factor 2 error in the originally published values was found (see supporting information, SI). We focus on the active measurements (the passive observations will be the subject of a following paper) and what they tell us about the geological history of Saturn's icy moons and their interaction with their near environment and, in particular, Saturn's dust rings.

2. Cassini Radar Observations of Saturn's Moons: Final Disk-Integrated 2.2-cm Radar Albedos

Measurements performed in the active mode operation of the Cassini RADAR give access to the disk-integrated 2.2-cm radar albedo of the targeted moon which is a measure of how reflective the surface of the target's visible hemisphere is in the backscatter direction compared to a reference surface. More specifically, the radar albedo is a dimensionless quantity derived by normalizing the radar cross section of a target by its projected geometric area. As stated in Ostro et al. (2010), the radar cross section of a target is "the projected area of a perfectly reflective, isotropic scatterer which, if observed at the target's distance from the RADAR with the same transmitted and received polarizations, would return the observed echo power." By definition, a perfectly reflective and isotropic surface (such as a smooth metallic sphere) has a radar albedo of 1. The radar albedo of a surface can exceed unity if the surface or, more accurately, if the depths probed at the operating wavelength, are such that the radar waves are preferentially scattered back toward their source (i.e., in the backscatter direction). The Cassini RADAR receives echoes in the same linear polarization as it transmits so it provides same-linear radar albedos at 2.2 cm. For more details, see Ostro et al. (2006, 2010), Wye (2011), and SI.

During the Cassini mission, the RADAR performed a total of 97 distant active observations also called "active stares." The list and geometry of these long-range observations are reported in Table S1. Rhea was the most examined satellite (26, +5 compared to Ostro et al., 2010) followed by Dione (18, +1), Iapetus (18), Enceladus (10, +3), Mimas (4, +1), Tethys (3), Hyperion (2), and Phoebe (2). Titan was also stared 8 times. The observations of Hyperion required a shape model; they were not reassessed in this work and six stare observations of a different kind on Dione and Rhea remain to be reduced (SI).

In addition to distant measurements, active spatially resolved data were acquired during one close flyby of Iapetus (Le Gall et al., 2014; Wye, 2011), two close flybys of Enceladus (one partially remaining to be analyzed; Wye, 2011; Le Gall et al., 2017), one close flyby of Rhea (Wye, 2011, reanalyzed for this work, SI) and one close flyby of Dione (this work, SI). These observations also provide estimates of regional 2.2-cm radar albedos that can be added to the analysis. The derivation of the radar albedos from both distant and targeted observations is described in the SI.

Figure 1a results from the reduction of 89 distant observations of the Saturnian moons, including Titan but not including Hyperion, and 4 spatially resolved active scans. It shows significant variations among the satellites with Enceladus having the highest average radar albedo (2.97 $\pm$0.35) and Titan the lowest (0.19 $\pm$0.06). All of Saturn's inner moons have extremely high radar albedos with values above unity even when accounting for all possible sources of uncertainties (SI). We note a trend toward a decrease in radar brightness from Enceladus outward with the exception of Rhea, unless it is Dione that is darker than expected. The implications of such findings and the satellite-to-satellite variability in term of radar albedo are further discussed below.

In Figure 1b observations centered on the leading side (centered at $-90°$E) of the satellites have been separated from observations collected on the trailing side (centered at 90°E) in order to explore potential hemispheric dichotomies. As already discussed in Ostro et al. (2010) and Le Gall et al. (2014), Iapetus's 2.2-cm

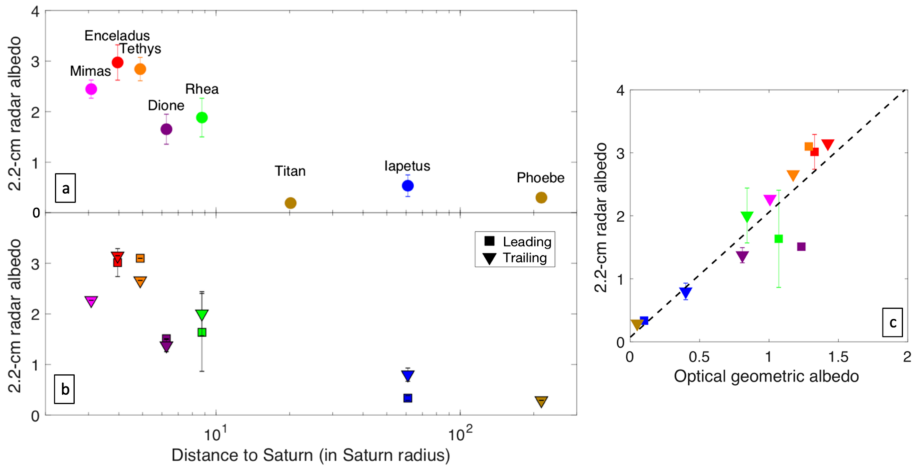

Figure 1. (a) Averaged 2.2-cm disk-integrated radar albedos of Saturn's major satellites. The error bars show the dispersion of the data set for each satellite. The statistical uncertainties on the derived albedos (inferred from the goodness of the fit; supporting information) are smaller than the size of the symbols. (b) Average 2.2-cm disk-integrated radar albedos measured on the leading and trailing hemispheres of each of Saturn's satellites. Note that the large error bar for Rhea's leading hemisphere is due to the strong contrast between the radar-bright ejecta blanket of the Inktomi crater and the radar-darker rest of Rhea's leading side. (c) Optical geometric versus 2.2-cm radar albedos. The optical geometric albedos are from Verbiscer et al. (2007; see also Hendrix et al., 2018) up to Rhea. Those for Iapetus and Phoebe are from Morrison et al. (1986). The best linear fit between these quantities is indicated (black dashed line); it relates the optical geometric albedo p to the 2.2-cm radar albedos A_{SL-2} as follows: $A_{SL-2} = 1.98p+0.07$.

radar albedo distribution mimics the dramatic two-tone optical coloration of the moon, Iapetus's leading hemisphere being significantly darker than its trailing hemisphere. In addition, hints of hemispheric dichotomies are found on Tethys, Dione, and maybe Rhea. The leading/trailing difference on Dione is strongly supported by the spatially resolved observation of this moon (Figures 2a and S3). On Rhea, the presence of the radar-bright fresh ejecta of the young crater Inktomi on the leading side (Figure 2b) reduces the significance of the hemispheric dichotomy (if any) but there seems to be a trend opposite to the case of Dione: Rhea's leading side is slightly darker than its trailing side (Figures 1b and S2). The evidence for a hemispheric dichotomy on Tethys is based on a much smaller number of observations but acquired with subspacecraft points and beam widths that encompass perfectly the two opposite hemispheres (Figure S2). There are not enough available observations to conclude for Mimas and no

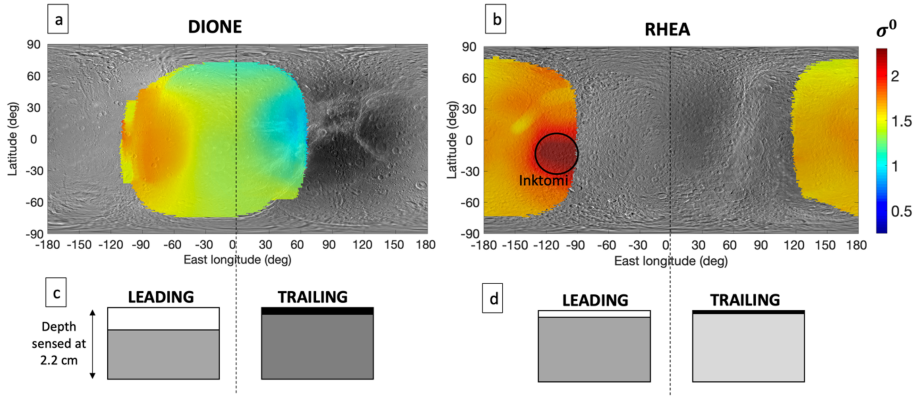

Figure 2. (a and b) Normalized backscattering cross sections σ^0 (corrected to an incidence angle of 32°) measured during Flybys DI163 and RH127, respectively (SI), overlaid on global mosaics composed of Cassini Imaging Science Subsystem images (Schenk et al., 2011). The black circle indicates Inktomi crater ejecta blanket. (c and d) Simplified models of the variations with depth of the degree of purity of the regoliths of Dione's and Rhea's leading and trailing hemispheres. The white layer on both leading hemispheres represents water ice particles from the E-ring while the top layers of the trailing sides seems to be covered by optically dark dust.

obvious leading/trailing radar albedo dichotomy on Enceladus, contrary to what is observed in the passive mode of operation of the Cassini RADAR, which has revealed a large-scale emissivity anomaly on the leading side of the satellite (Ries & Janssen, 2015). Figure 1c is discussed in the following section.

3. Discussion

3.1. A Measure of the Degree of Purity of the Water Ice Regolith

It is commonly acknowledged that the microwave signatures of ice-rich satellites of both the Jovian and Saturnian systems are dominated by volume and multiple scatterings within their extremely low loss and structurally complex regoliths (Black et al., 2001; Hapke, 1990; Janssen et al., 2009; Ostro, 1993; Ostro et al., 2006, 2010; Zebker et al., 2008). The shapes of the echo spectra from which were derived the radar albedos of Saturn's moons are consistent with this understanding; they are typical of purely diffuse scattering, that is, very broad with no trace of a central specular peak (Ostro et al., 2006, 2010; Figure S1b).

Volume and multiple scatterings are caused by heterogeneities in the subsurface such as embedded dielectric inclusions or interfaces (rocks, voids, cracks, ... Black et al., 2001; Goldstein & Green, 1980; Hagfors et al., 1997, 1985). High-order scattering from these heterogeneities is favored by a large penetration depth of the microwaves into the subsurface. The high transparency of cold water ice to radio wavelengths indeed guarantees a large penetration depth of the incident waves (as large as tens or even hundreds of wavelengths; e.g., Lorenz, 1998; Maetzler, 1998; Thompson & Squyres, 1990), which have therefore more opportunities to be scattered back to their direction of arrival (i.e., to the radar, in the backscattering direction). The purer the water ice regolith, the larger the backscatterer it is expected to produce.

Consistently, the ejecta blanket of the young Inktomi crater on Rhea where ultraclean native water ice has been excavated (Scipioni et al., 2014; Stephan et al., 2012) and exposed at the near surface is especially radar bright (Figure 2b). Conversely, on Dione, the optically dark trailing hemisphere is depleted in water ice (Scipioni et al., 2013; Stephan et al., 2010) and radar-dark. At first order, the radar albedos of Saturn's moons can therefore be regarded as a measure of the degree of purity of their regoliths or, inversely, as a measure of their degree of contamination by non-ice compounds.

A further argument for this assertion is the strong positive correlation between the 2.2-cm radar albedos of Saturn's moons and their visual geometric albedo (Figure 1c; Ostro et al., 2006, 2010). The visual geometric albedo is a measure of how well the surface reflects the light back in the direction of illumination (i.e., the Sun) compared to an idealized isotropic surface. As such, it can also exceed unity when the surface is especially efficient at retro-reflecting the light and it is a quantity more relevant to compare to the radar albedo than the Bond bolometric albedo.

Figure 1c shows the almost perfect linear positive correlation between the optical geometric and radar albedos (with a Pearson correlation coefficient of 0.91); it strongly points to the idea that an increasing concentration of optically dark contaminant(s) in the near surface leads to the attenuation of the high-order scattering in the subsurface and thus to smaller radar albedos. This further implies that (i) the regolith contaminants are both optically dark and microwave absorbing, (ii) the contaminants at the uppermost part of the surface are similar in composition to those at the depths sensed at 2.2-cm wavelength, that is, several decimeters or even few meters below the surface, and (iii) the subsurface/surface contaminant ratio is constant among most satellites. This is likely made possible by impact gardening which brings exogenic contaminants to the subsurface (Cooper et al., 2001).

However, we note that the correlation seen in Figure 1c somewhat diverts from the general trend for the leading sides of both Dione and Rhea suggesting that the subsurfaces of these hemispheres are more contaminated by impurities than their very surfaces compared to other satellites and their trailing hemispheres. On Dione, the subsurface of the leading side, like the surface, is nevertheless cleaner than that of the trailing side while it may be the reverse on Rhea where observations suggest a possible opposite correlation between the optical and radar albedos. Based on these observations (which are further discussed in the following section), Figures 2c and 2d propose simplified models of the variations with depth of the degree of purity of the regoliths of Dione and Rhea, respectively. In these models, underlying a snow or dust cover, the water ice subsurface of Rhea is equally pure or purer than that of Dione. Both the snow and dust covers of Rhea's leading and trailing sides, respectively, are thinner than those of Dione.

3.2. Processes Controlling the Degree of Purity of Water Ice Regoliths in the Saturnian System

As discussed above, the intersatellite and intrasatellite variations of radar albedos shown in Figure 1 primarily reflect variations in terms of subsurface contamination by non-ice compounds. Titan is the dimmest of the radar targets, which is not surprising since its icy crust is covered—in most places—with a sedimentary layer composed of organic materials produced by photochemistry in the atmosphere (e.g., Janssen et al., 2016). For Saturn's atmosphere-less satellites, the degree of purity of the regolith is the result of the competition between several processes including (i) the interaction with Saturn's dust rings and in particular with the E-ring near the planet and the vast debris ring from Phoebe further away, (ii) the geological and thermal history of each satellite or, in other words, its surface age, (iii) the efficiency of space weathering at the position of the satellite in Saturn's system.

Exploring the hemispheric dichotomies can help diagnose the major processes at play in the near surface (as all of Saturn's major satellites have synchronous orbits). For instance, dynamical models predict that low-reflectivity materials from the diffuse debris ring around Phoebe should be progressively deposited on the leading side of Iapetus. This is the most likely explanation for Iapetus's dramatic hemispheric dichotomy (e.g., Buratti et al., 2002; Cruikshank et al., 1983; Spencer & Denk, 2010; Tamayo et al., 2011; Tosi et al., 2010; Verbiscer et al., 2009). As a further argument, the radar albedo of Iapetus's leading side is exactly the same as that of Phoebe (Figure 1b). The dark contaminant must be present at depths of at least a few decimeters otherwise the hemispheric dichotomy of Iapetus would not be visible at a wavelength of 2.2 cm. On the other hand, the thickness of the dark exogenic layer must be at most a few meters since observations from the Arecibo radar system at 12.6-cm wavelength show no longitudinal pattern (Black et al., 2004; Le Gall et al., 2014; Ostro et al., 2006, 2010). This is consistent with predictions from dynamical models of dust deposition (Tamayo et al., 2011) and infrared observations (Rivera-Valentin et al., 2011).

Inversely, closer to Saturn, Mimas, Enceladus, Tethys, Dione, and Rhea are engulfed in the E-ring, which is fed by Enceladus' plume (Kempf et al., 2010) and guarantees the deposition at their surface of particles of extremely pure water ice (Hillier et al., 2007; Verbiscer et al., 2007). The interaction of Saturn's inner moons with the E-ring is further discussed in the next section as it is believed to be a major process controlling their radar brightness.

Another way to bring fresh and clean water ice in the near surface of icy moons is recent—or current—geological activity. This may, at least partially, explain the extreme radar brightness of Enceladus and, to a lesser extent, the brighter leading side of Dione, which is covered by smooth terrains (Schenk & Moore, 2009) and must have a long resurfacing history (Kirchoff & Schenk, 2015). In the case of Enceladus, we recall that while 2.2-cm active observations show no clear leading/trailing asymmetry (Figure 1b), passive observations, both unresolved and resolved, do; the leading side of Enceladus is about 30% less emissive than its surrounding terrains (Ries & Janssen, 2015). A consistent dichotomy is observed in Arecibo 13-cm measurements, which reveal a much brighter leading side (Black et al., 2007). Ries and Janssen (2015) propose that the leading side anomaly is associated to a seemingly young tectonized terrain mapped by Crow-Willard and Pappalardo (2015) and called the Leading Hemisphere Terrain (LHT). In this picture, the LHT would be young enough (<200 Myr) to have been reprocessed (e.g., by micrometeoritic bombardment) only down to a depth shallower than the electrical skin depth at 2.2 cm (a few meters at most) contrary to the trailing side. This would be the reason why the leading/trailing dichotomy is not visible in 2.2-cm active data which probe the subsurface down to smaller depths than concurrent passive measurements (two-way versus one-way attenuations) and radio observations at 13 cm. In addition, or alternatively, at the depth sensed by the Cassini RADAR in active mode, the coating effect of the falling particles from the plume and the E-ring (Kempf et al., 2010, 2018) could balance or prevail on both hemispheres over the brightness of the underlying young LHT.

Lastly, variations in the level of cleanliness of the near surface can reflect differences in the space weathering environment. For instance, close to Saturn, gravitational focusing enhances the meteoroid flux, which should lead to a faster contamination by non-ice compounds. Bombardment by charged particles can also alter chemically (and structurally) the uppermost layers of the regolith of Saturn's moons depending on their position inside Saturn's magnetosphere (e.g., the “Pac-Men” revealed by Cassini's Composite Infrared Spectrometer on the leading sides of Mimas and Tethys, which are thermally anomalous and ultraviolet dark regions coinciding, in shape and location, with regions of preferential bombardment by high-energy electrons; Howett et al., 2011; Howett et al., 2012). The assessment of the effects of the different agents of

space weathering (dust, photons, low- and high-energy particles, neutral particles, temperature variations, ...) on the albedo of a water ice regolith is not straightforward and out of scope of this paper. However, we note that Scipioni et al. (2014) advance that the enhanced brightness of Rhea could be related to the weaker efficiency of space weathering at the location of its orbit, far from the most intense radiation belts of Saturn. Indeed, Rhea is surprisingly brighter than Dione in the infrared (Scipioni et al., 2014) as well as at 2.2-cm (Figures 1 and 2) and at 13-cm wavelengths (Black et al., 2007), whereas it is further away from the source of the E-ring and seemingly less endogenically evolved (e.g., Kirchoff et al., 2018). Alternatively, Ostro et al. (2010) propose that Rhea's enhanced brightness compared to Dione could be due to an older and thus more well-structured regolith, with heterogeneities able to produce a more efficient volume scattering. We rather favor the first hypothesis since it appears that the least matured (i.e., the youngest) terrains in the Saturnian system (e.g., Enceladus's south pole the ejecta blanket of crater Inktomi on Rhea) are also the radar-brightest. Consistently, there is evidence that Dione's terrains (in particular its trailing side) are more contaminated by an unidentified exogenic darkening agent than Rhea (Figure 2; Clark et al., 2008).

3.3. E-Ring Coating of the Surface of Saturn's Inner Moons

The almost perfect correlation between the radar and optical geometric albedos (Figure 1c) points to the key role of the E-ring grain coating in the radar brightness of Saturn's moons. Indeed, Verbiscer et al. (2007) establish that the optical geometric albedos of Saturn's inner satellites follow the reflectance profile of the E-ring as a function of the distance from the planet. Likewise, the overall decrease in radar brightness from Enceladus outward is likely related to the outward decrease in E-ring flux.

The dynamic of the E-ring particles is driven by the combined effects of gravity, radiation pressure, drag, and electromagnetic forces (e.g., Horányi et al., 2008). Their relative influx and deposition pattern at the surface of each inner moon (Juhász & Horányi, 2015; Kempf et al., 2018) could explain not only the sequence of radar albedos in Saturn's system but also some of the observed hemispheric dichotomies as a result of differential accumulation of E-ring material. Indeed, the region most heavily bombarded by ultrapure water ice from the E-ring is the trailing side of the innermost Mimas (see also Hamilton & Burns, 1994) while it shifts to the leading side for the moons outward Enceladus' orbit. This is the most likely cause of the brightening of these hemispheres on Tethys and, to a lesser extent, on Dione at both visible and microwave wavelengths. The case of Enceladus is more complicated since the amount of snow grains falling back directly from the jets largely prevail over the deposition of E-ring particles (Kempf et al., 2010). In the case of Rhea, the Cassini RADAR probably probes well below the E-ring deposition layer hence the opposite (or lack of) correlation between the optical and radar albedos (Figure 1c).

At least a few decimeters of E-ring material are required to guarantee a significant effect on the degree of scattering in the subsurface volume at 2.2 cm and hence on the measured radar albedos (e.g., Black et al., 2001). However, current models predict much thinner deposits. Based on Hendrix et al. (2018); which refers to Juhász & Horányi, 2015) and assuming a porosity of 50%, a layer of at best a few centimeters (a few centimeters for Mimas, less than a centimeter for Tethys, less than a millimeter for Dione and Rhea) of E-ring material should mantle the surfaces of Saturn's inner moons after 100 Myr (a likely strict upper limit for the age of the E-ring and cryovolcanism on Enceladus; e.g., Kargel, 2006; Roberts & Nimmo, 2008).

The discrepancy between model predictions of E-ring influx and observations has already been reported by Hirata et al. (2014); based on the analysis of depositional features on Helene (a co-orbital moon of Dione), they estimate the E-ring deposits to be tens to hundreds of meters thick. The E-ring snow cover on Saturn's inner middle-sized moons is visibly not as thick as on this small satellite; nevertheless, Cassini RADAR observations strongly suggest that the models are underestimating it, at least for the innermost moons Mimas, Tethys, and Dione. This also holds true for Enceladus where evidence for buried craters (Kirchoff & Schenk, 2009) and pit chains (Martin et al., 2017) point to a much thicker regolith than predicted by models of plume-sourced regolith deposition.

3.4. Structure of the Regoliths

The radar albedos measured in the Saturnian innermost system are significantly greater than those of the Galilean satellites (Table S2), which suggests cleaner regoliths. However, while it is clear that the degree of purity of the water ice regolith controls the significance of high-order scattering in the near surface, the composition alone cannot explain the extremely high albedos recorded by the Cassini RADAR as well as

the lack of a specular component in the echo spectra. The "snow cover" of Saturn's icy moons must contain scattering structures that are especially efficient in returning waves in the backscattering direction.

In order to explain the high radar returns from Jupiter's satellites, some authors invoke refraction onto exotic or "ordered" scattering structures such as buried ice channels (or "ice pipes" like those found in the percolation zones of the Greenland ice shelf; Rignot et al., 1993; Rignot, 1995), large spheroidal or piece of spheroidal inclusions with a refractivity index profile that progressively bent the rays toward the backscattering direction ("Maxwell's fish eye" lens-like structures, Hagfors et al., 1985, 1997) or buried craters (Eshleman, 1986). However, such structures or the mechanisms that could produce them on Saturn's satellites remain to be identified.

Other theories rely on the coherent backscatter effect (CBE; Hapke, 1990; Peters, 1992; Black et al., 2001), which results from the constructive interferences of waves in the backscattering direction after a multiplicity of random scattering events. Such an effect is expected in presence of wavelength-scale scatterers embedded in a weakly absorbing regolith and is all the more efficient as scatterers are themselves made of low-loss material, that is, void or pure ice (Black et al., 2001). Scatterers are not necessarily spherical inclusions but could be fractures or cracks induced by impacts or thermal stress.

The CBE model is geologically plausible and proved to be able to explain the radar albedos of the Galilean moons (Black et al., 2001). However, its capacity to boost the intensity in the backscattering direction is limited and an extremely high density of scatterers (as much as 80% of the scattering layer must be occupied by scatterers) is already required for Europa, the brightest of these satellites which is equivalent in term of total-power radar albedo to Dione but twice as faint as Enceladus (Table S2). Future works will have to demonstrate the ability of this model to reproduce the even higher Cassini measurements or propose other explanations.

4. Conclusion

To conclude, Saturn's inner moons are especially bright at 2.2-cm wavelength. Whether it is due to random scattering or refraction on (and into) organized structures, the extremely high radar albedos measured by the Cassini RADAR point to the high degree of purity of the water ice regoliths in Saturn's inner system. Further, they suggest that Saturn's innermost moons have cleaner ice shells than that of the Galilean moons.

Based on the intervariations and intravariations of radar albedos in the Saturn's system, youth rather than maturity seems to guarantee high radar brightness, which could bring another argument for the theory that the middle-sized satellites of Saturn are younger than previously thought (e.g., Canup & Ward, 2006). Indeed, recent Cassini results on the incoming flux of meteoroid-dust near Saturn suggests that the rings and the suite of inner moons that likely emerged from them (Mimas, Enceladus, Tethys, Dione, and Rhea; Charnoz et al., 2011) could be as young as 100–200 Myr (Cuzzi, 2018; Kempf et al., 2017). This scenario relies on the very same idea that the rings would not be so bright (i.e., clean) if they were older and is supported by the new determination of Saturn's effective tidal dissipation (Lainey et al., 2017).

On the other hand, most Cassini measurements can be explained by the interaction of the satellites with Saturn's main dust rings, namely, the E-ring and the Phoebe ring. In particular, the apparent youthfulness of the innermost moons at radar wavelength is likely the result of the deposition of at least a few decimeters of fresh and clean "snow" from the E-ring (and plume fallback in the case of Enceladus). This, in turn, raises the question of the intensity and age of Enceladus's cryovolcanic activity and suggests that current models underestimate the rate of deposition of particles from the E-ring at the surface of Enceladus's neighbors.

It remains to determine which scattering structures cause the high recorded radar returns. On Enceladus, a variety of surface and subsurface features have been observed (e.g., ice blocks and pinnacles; Helfenstein & Porco, 2015) or can be envisioned as the result of some combination of sublimation and ablation related to the south pole geyser activity. However, on the other moons, the most common mechanism acting on the overall regolith evolution down to decimeters/meters depth is probably thermal stress. A dense collection of random centimetric fractures would lead to an efficient CBE (Black et al., 2001), but it has not been demonstrated yet that it could explain the especially high radar albedos recorded in the Saturn's inner system.

Alternatively, the water ice surface of Saturn's innermost moons could be sculpted into exotic structures such as penitentes (as recently proposed for Europa, Hobley et al., 2018) or Sun cups (as observed on Hyperion), which could act as efficient retroreflectors. However, it remains to prove that the sublimation rate is

sufficiently high in the Saturn system to form such structures and to determine which dimension and spacing between them are required to produce the radar returns of the magnitudes observed.

Cassini radar observations, and more generally microwave observations, therefore hold key insights into both the composition and structure of the near surface of Saturn's moons. As such, they contain clues to better understand the evolution of these objects and, in particular, their interaction with Saturn's unique ring environment. They also provide important constraints to prepare future missions to icy satellites, especially those including a lander.

Acknowledgments
The authors wish to thank the Cassini-Huygens team for the design, development, and operation of the mission. The Cassini- Huygens mission was a joint endeavor of NASA, ESA, and ASI and managed by JPL/Caltech under a contract with NASA. The authors also are especially grateful to Cassini's Satellite Orbiter Science Team (SOST) and in particular to Steve Ostro, Rosaly Lopes, Karl Mitchell, Yanhua Anderson, Ralph Lorenz, and Mike Janssen in the planning and design of the Cassini RADAR icy satellite observations. A. L. G. is supported by the IUF (Institut Universitaire de France). L. E. B. is supported by the Région Ile-de-France (DIM-ACAV). The radar data used are available on PDS (Planetary Data System) as LBDR (Long Burst Data Records, i.e., instrument telemetry and calibrated science data in burst order; http://pds-imaging.jpl.nasa.gov/volumes/radar.html).

References

Black, G. J., Campbell, D. B., & Carter, L. M. (2007). Arecibo radar observations of Rhea, Dione, Tethys, and Enceladus. *Icarus*, *191*(2), 702–711. https://doi.org/10.1016/j.icarus.2007.06.009

Black, G. J., Campbell, D. B., Carter, L. M., & Ostro, S. J. (2004). Radar detection of Iapetus. *Science*, *304*(5670), 553. https://doi.org/10.1126/science.1096470

Black, G. J., Campbell, D. B., & Nicholson, P. D. (2001). Icy Galilean satellites: Modeling radar reflectivities as a coherent backscattering effect. *Icarus*, *151*, 167–180.

Buratti, B. J., Hicks, M. D., Tryka, K. A., Sittig, M. S., & Newburn, R. L. (2002). High-resolution 0.33–0.92 μm spectra of Iapetus, Hyperion, Phoebe, Rhea, Dione, and D-type asteroids: How are they related? *Icarus*, *155*, 375–381.

Canup, R. M., & Ward, W. R. (2006). A common mass scaling for satellite systems of gaseous planets. *Nature*, *441*(7095), 834–839. https://doi.org/10.1038/nature04860

Charnoz, S., Crida, A., Castillo-Rogez, J. C., Lainey, V., Dones, L., Karatekin, O., et al. (2011). Accretion of Saturn's mid-sized moons during the viscous spreading of young massive rings: Solving the paradox of silicate-poor rings versus silicate-rich moons. *Icarus*, *216*(2), 535–550.

Clark, R. N., Curchin, J. M., Jaumann, R., Cruikshank, D. P., Brown, R. H., Hoefen, T. M., et al. (2008). Compositional mapping of Saturn's satellite Dione with Cassini VIMS and implications of dark material in the Saturn system. *Icarus*, *193*(2), 372–386. https://doi.org/10.1016/j.icarus.2007.08.035

Clark, R. N., Fanale, F. P., & Gaffey, M. J. (1986). Surface composition of natural satellites. In J. A. Burns & M. S. Matthews (Eds.), *Satellites* (pp. 437–491). Tucson: University of Arizona Press.

Cooper, J. F., Johnson, R. E., Mauk, B. H., Garrett, H. B., & Gehrels, N. (2001). Energetic ion and electron irradiation of the icy Galilean satellites. *Icarus*, *149*, 133–159.

Crow-Willard, E. N., & Pappalardo, R. T. (2015). Structural mapping of Enceladus and implications for formation of tectonized regions. *Journal of Geophysical Research: Planets*, *120*, 928–950. https://doi.org/10.1002/2015JE004818

Cruikshank, D. P., Bell, J. F., Gaffey, M. J., Brown, R. H., Howell, R., Beerman, C., & Rognstad, M. (1983). The dark side of Iapetus. *Icarus*, *53*, 90–104.

Cuzzi, J. N. (2018). Saturn's rings after Cassini, LPSC, #2083

Eshleman, V. R. (1986). Radar glory from buried craters on icy moons. *Science*, *234*(4776), 587–590. https://doi.org/10.1126/science.234.4776.587

Goldstein, R. M., & Green, R. R. (1980). Ganymede: Radar surface characteristics. *Science*, *207*, 179–180. https://doi.org/10.1126/science.207.4427.179

Hagfors, T., Dahlstrom, I., Gold, T., Hamran, S.-E., & Hansen, R. (1997). Refraction scattering in the anomalous reflections from icy surfaces. *Icarus*, *130*(2), 313–322. https://doi.org/10.1006/icar.1997.5844

Hagfors, T., Gold, T., & Ierkic, H. M. (1985). Refraction scattering as origin of the anomalous radar returns of Jupiter's satellites. *Nature*, *315*, 637–640.

Hamilton, D. P., & Burns, J. A. (1994). Origin of Saturn's E ring: Self-sustained, naturally. *Science*, *264*, 550–553. https://doi.org/10.1126/science.264.5158.550

Hapke, B. (1990). Coherent backscatter and the radar characteristics of outer planet satellites. *Icarus*, *88*, 407–417.

Helfenstein, P., & Porco, C. C. (2015). Enceladus' geysers: Relation to geological features. *The Astronomical Journal*, *150*(3).

Hendrix, A. R., Filacchione, G., Paranicas, C., Schenk, P., & Scipioni, F. (2018). Icy Saturnian satellites: Disk-integrated UV-IR characteristics and links to exogenic processes. *Icarus*, *300*, 103–114.

Hillier, J. K., Green, S. F., McBride, N., Schwanethal, J. P., Postberg, F., Srama, R., et al. (2007). The composition of Saturn's E ring. *Monthly Notices of the Royal Astronomical Society*, *377*(4), 1588–1596.

Hirata, N., Miyamoto, H., & Showman, A. P. (2014). Particle deposition on the Saturnian satellites from ephemeral cryovolcanism on Enceladus. *Geophysical Research Letters*, *41*, 4135–4141.

Hobley, D. E. J., Moore, J. M., Howard, A. D., & Umurhan, O. M. (2018). Formation of metre-scale bladed roughness on Europa's surface by ablation of ice. *Nature Geoscience*, *11*, 901–904.

Horányi, M., Juhász, A., & Morfill, G. E. (2008). Large-scale structure of Saturn's E-ring. *Geophysical Research Letters*, *35*, L04203. https://doi.org/10.1029/2007GL032726

Howett, C. J. A., Spencer, J. R., Hurford, T. A., Verbiscer, A., & Segura, M. (2012). PacMan returns: An electron-generated thermal anomaly on Tethys. *Icarus*, *221*(2), 1084–1088. https://doi.org/10.1016/j.icarus.2012.10.013

Howett, C. J. A., Spencer, J. R., Schenk, P., Johnson, R. E., Paranicas, C., Hurford, T. A., et al. (2011). A high-amplitude thermal inertia anomaly of probable magnetospheric origin on Saturn's moon Mimas. *Icarus*, *216*, 221–226.

Janssen, M. A., Le Gall, A., Lopes, R. M., Lorenz, R. D., Malaska, M. J., Hayes, A. G., et al. (2016). Titan's surface at 2.18-cm wavelength imaged by the Cassini RADAR radiometer: Results and interpretations through the first ten years of observation. *Icarus*, *270*, 443–459. https://doi.org/10.1016/j.icarus.2015.09.027

Janssen, M. A., Lorenz, R. D., West, R., Paganelli, F., Lopes, R. M., Kirk, R. L., et al., & the Cassini Radar Team (2009). Titan's surface at 2.2-cm wavelength imaged by the Cassini RADAR radiometer: Calibration and first results. *Icarus*, *200*, 222–239.

Juhász, A., & Horányi, M. (2015). Dust delivery from Enceladus to the moons of Saturn. American Geophysical Union, Abstract 77479.

Kargel, J. S. (2006). Perspective—Enceladus: Cosmic gymnast, volatile miniworld. *Science*, *311*(5766), 1389–1391. https://doi.org/10.1126/science.1124495

Kempf, S., Altobelli, N., Srama, R., Cuzzi, J. N., & Estrada, P. R. (2017). The age of Saturn's rings constrained by the meteoroid flux into the system, American Geophysical Union, Fall Meeting 2017, abstract #P34A-05

Kempf, S., Beckmann, U., & Schmidt, J. (2010). How the Enceladus dust plume feeds Saturn's E ring. *Icarus*, *206*, 446–457.
Kempf, S., Horányi, M., Hsu, H.-W., Hill, T. W., Juhász, A., & Smith, H. T. (2018). Saturn's diffuse E ring and its connection with Enceladus. In P. M. Schenk, et al. (Eds.), *Enceladus and the Icy Moons of Saturn* (pp. 195–210). Tucson: University of Arizona.
Kirchoff, M. R., Bierhaus, E. B., Dones, L., Robbins, S. J., Singer, K. N., Wagner, R. J., & Zahnle, K. J. (2018). Cratering histories in the Saturnian system. In P. M. Schenk, et al. (Eds.), *Enceladus and the Icy Moons of Saturn* (pp. 267–284). Tucson: University of Arizona.
Kirchoff, M. R., & Schenk, P. (2015). Dione's resurfacing history as determined from a global impact crater database. *Icarus*, *256*, 78–89.
Kirchoff, M. R., & Schenk, P. (2009). Crater modification and geologic activity in Enceladus' heavily cratered plains: Evidence from the impact crater distribution. *Icarus*, *202*(2), 656–668.
Lainey, V., Jacobson, R. A., Tajeddine, R., Cooper, N. J., Murray, C., Robert, V., et al. (2017). New constraints on Saturn's interior from Cassini astrometric data. *Icarus*, *281*(1), 286–296. https://doi.org/10.1016/j.icarus.2016.07.014
Le Gall, A., Leyrat, C., Janssen, M. A., Choblet, G., Tobie, G., Bourgeois, O., et al. (2017). Thermally anomalous features in the subsurface of Enceladus's south polar terrain. *Nature Astronomy*, *1-0063*.
Le Gall, A., Leyrat, C., Janssen, M. A., Keihm, S., Wye, L. C., West, R., et al. (2014). Iapetus' near surface thermal emission modeled and constrained using Cassini RADAR Radiometer microwave observations. *Icarus*, *241*, 221–238.
Lorenz, R. D. (1998). Preliminary measurements of the cryogenic dielectric properties of water–ammonia ices: Application to radar observations of icy satellites. *Icarus*, *136*, 344–348.
Maetzler (1998). In B. Schmitt, C. DeBergh, & M. Festou (Eds.), *Solar system ices* (pp. 241–257). Dordrecht: Kluwer Academic.
Martin, E. S., Kattenhorn, S. A., Collins, G. C., Michaud, R. L., Pappalardo, R. T., & Wyrick, D. Y. (2017). Pit chains on Enceladus signal the recent tectonic dissection of the ancient cratered terrains. *Icarus*, *294*, 209–217.
Morrison, D., Owen, T., & Soderblom, L. (1986). The satellites of Saturn. In J. A. Burns & M. S. Matthews (Eds.), *Satellites* (pp. 764–801). Tucson: University of Arizona Press.
Ostro, S. J. (1993). Planetary radar astronomy. *Reviews of Modern Physics*, *65*(4), 1235–1279. https://doi.org/10.1103/RevModPhys.65.1235
Ostro, S. J., West, R. D., Janssen, M. A., Lorenz, R. D., Zebker, H. A., Black, G. J., et al. (2006). Cassini RADAR observations of Enceladus, Tethys, Dione, Rhea, Iapetus, Hyperion, and Phoebe. *Icarus*, *183*(2), 479–490. https://doi.org/10.1016/j.icarus.2006.02.019
Ostro, S. J., West, R. D., Wye, L. C., Zebker, H. A., Janssen, M. A., Stiles, B., et al., & the Cassini Radar Team (2010). New Cassini RADAR results for Saturn's icy satellites. *Icarus*, *206*(2), 498–506. https://doi.org/10.1016/j.icarus.2009.07.041
Peters, K. (1992). The coherent backscatter effect: A vector formulation accounting for polarization and absorption effects and small or large scatterers. *Physical Review B*, *46*(2), 801–812. https://doi.org/10.1103/PhysRevB.46.801
Porco, C. C., Helfenstein, P., Thomas, P. C., Ingersoll, A. P., Wisdom, J., West, R., et al. (2006). Cassini observes the active south pole of Enceladus. *Science*, *311*(5766), 1393–1401. https://doi.org/10.1126/science.1123013
Ries, P. A., & Janssen, M. A. (2015). Large-scale anomaly in Enceladus microwave emission. *Icarus*, *257*, 88–102. https://doi.org/10.1016/j.icarus.2015.04.030
Rignot, E. (1995). Backscatter model for the unusual radar properties of the Greenland Ice Sheet. *Journal of Geophysical Research*, *100*(E5), 9389–9400. https://doi.org/10.1029/95JE00485
Rignot, E., Ostro, S. J., Van Zyl, J. J., & Jezek, K. C. (1993). Unusual radar echoes from the Greenland ice sheet. *Science*, *261*(5129), 1710–1713. https://doi.org/10.1126/science.261.5129.1710
Rivera-Valentin, E. G., Blackburn, D. G., & Ulrich, R. (2011). Revisiting the thermal inertia of Iapetus: Clues to the thickness of the dark material. *Icarus*, *216*, 347–358.
Roberts, J. H., & Nimmo, F. (2008). Tidal heating and the long-term stability of a subsurface ocean on Enceladus. *Icarus*, *194*(2), 675–689.
Schenk, P., Hamilton, D. P., Johnson, R. E., McKinnon, W. B., Paranicas, C., Schmidt, J., & Showalter, M. R. (2011). Plasma, plumes and rings: Saturn system dynamics as recorded in global color patterns on its midsize icy satellites. *Icarus*, *211*(1), 740–757. https://doi.org/10.1016/j.icarus.2010.08.016
Schenk, P. M., & Moore, J. M. (2009). *Eruptive volcanism on Saturn's icy moon Dione*, (2465). Woodlands, Texas: Lunar Planetary Science XL.
Scipioni, F., Tosi, F., Stephan, K., Filacchione, G., Ciarniello, M., Capaccioni, F., & Cerroni, P. (2014). The VIMS Team Spectroscopic classification of icy satellites of Saturn I: Identification of terrain units on Dione. *Icarus*, *243*, 1–16.
Scipioni, F., Tosi, F., Stephan, K., Filacchione, G., Ciarniello, M., Capaccioni, F., Cerroni, P., & VIMS Team (2013). Spectroscopic classification of icy satellites of Saturn I: Identification of terrain units on Dione. *Icarus*, *226*, 1331–1349.
Spencer, J. R., & Denk, T. (2010). Formation of Iapetus' extreme albedo dichotomy by exogenically triggered thermal ice migration. *Science*, *327*(5964), 432–435. https://doi.org/10.1126/science.1177132
Stephan, K., Jaumann, R., Wagner, R., Clark, R. N., Cruikshank, D. P., Giese, B., et al. (2012). The Saturnian satellite Rhea as seen by Cassini VIMS. *Planetary and Space Science*, *61*(1), 142–160. https://doi.org/10.1016/j.pss.2011.07.019
Stephan, K., Jaumann, R., Wagner, R., Clark, R. N., Cruikshank, D. P., Hibbitts, C. A., et al. (2010). Dione's spectral and geological properties. *Icarus*, *206*, 631–652.
Tamayo, D., Burns, J. A., Hamilton, D. P., & Hedman, M. M. (2011). Finding the trigger to Iapetus' odd global albedo pattern: Dynamics of dust from Saturn's irregular satellites. *Icarus*, *215*, 260–278.
Thompson, W. D., & Squyres, S. W. (1990). Titan and other icy satellites: Dielectric properties of constituent materials and implications for radar sounding. *Icarus*, *86*, 336–354.
Tosi, F., Turrini, D., Coradini, A., & Filacchione, G. (2010). Probing the origin of the dark material on Iapetus. *Monthly Notices of the Royal Astronomical Society*, *403*, 1113–1130.
Verbiscer, A., French, R., Showalter, M., & Helfenstein, P. (2007). Enceladus: Cosmic graffiti artist caught in the act. *Science*, *315*, 815.
Verbiscer, A. J., Skrutskie, M. F., & Hamilton, D. P. (2009). Saturn's largest ring. *Nature*, *461*, 1098.
Wye, L. (2011). Radar scattering from Titan and Saturn's icy satellites using the Cassini spacecraft, Ph.D. Thesis, Stanford University, Faculty of Engineering, 316.
Zebker, R. D., Wye, L. C., Janssen, M. A., & the Cassini Radar Team (2008). Titan's surface from reconciled Cassini microwave reflectivity and emissivity observations. *Icarus*, *194*, 704–710.

References From the Supporting Information

Zhang, Z., Hayes, A. G., Janssen, M. A., Nicholson, P. D., Cuzzi, J. N., de Pater, I., et al. (2017). Cassini microwave observations provide clues to the origin of Saturn's C ring. *Icarus*, *281*, 297–321.